Bionanofabrication of Ordered Nanoparticle Arrays: Effect of Particle Properties and Adsorption Conditions

Magnus Bergkvist,*,† Sonny S. Mark,† Xin Yang,‡ Esther R. Angert,† and Carl A. Batt‡

Department of Microbiology, Cornell University, Wing Hall, Ithaca, NY 14853, and Alliance for Nanomedical Technologies, Cornell University, Stocking Hall, Ithaca, NY 14853

Received: February 17, 2004; In Final Form: April 15, 2004

Arrays of Au nanoparticles were created using the inherent repeating patterns of bacterial S-layer proteins. Bacterial self-assembling S-layer protein lattices display a highly repetitive surface structure that makes them particularly suitable as biotemplates to fabricate metallic/semiconducting nanostructures and arrays. One interesting S-layer for nanoparticle templating is the hexagonally packed intermediate (HPI) layer of *Deinococcus radiodurans*. This S-layer, displaying hexagonal (p6) symmetry, is comprised of a hexameric protein core unit with a central pore, surrounded by six relatively large openings ("vertex points"). In this work, the influences of particle properties and adsorption conditions on the formation of ordered arrays of 5-nm Au nanoparticles using HPI S-layers were investigated. Using transmission electron microscopy (TEM), it was found that the templating of citrate-capped Au nanoparticles on HPI layers under low ionic strength conditions resulted in hexagonal-packed ordered arrays with ∼18-nm interparticle spacings that corresponded with the pore-to-pore distance of the S-layer. Interestingly, nanoparticle binding occurs at the vertex points on the HPI layer and, due to repulsion forces, adsorption tends to be favored at every second vertex point. Upon increasing the ionic strength, ordered packing is still observed. However, because interparticle repulsions are less prominent, adsorption of nanoparticles occurs in virtually every available vertex point, resulting in the formation of a honeycomb-like pattern of nanoparticles extending throughout the HPI monolayer sheet. Combined with the results of additional investigations using either uncharged hydroxy-terminated particles or positively charged ferritin molecules, the experimental data suggest that the creation of ordered arrays through biotemplating of Au nanoparticles onto HPI S-layers depends on the electrostatic interactions between individual nanoparticles as well as the interaction with the HPI layer.

Introduction

Creating structures and arrays on a nanoscale is of key interest not only in the electronics industry, to enable the production of smaller devices, but also for fundamental nanotechnology studies, to investigate nanoscale phenomena and novel electronic/optical properties.[1−3] As conventional photolithography techniques are pushed to their limits, new approaches to fabricate nanostructures are starting to emerge, such as the use of block copolymers, nanoparticle-based self-assembly/monolayer formation, and micelles for the creation of ordered nanoarrays.[4−10] In addition to these organic chemistry approaches, nature's own abilities to create ordered structures for the manufacture/assembly of artificial nanostructures can be exploited. DNA, for instance, has been used for the alignment and ordering of gold (Au) nanoparticles,[11−13] ferritin has been used to create arrays of nanoparticles,[14] and viruses have been used to arrange quantum dots[15] and nanowires[16] into ordered arrays. Although these methods can be useful for synthesizing ordered nanostructures, other types of proteins that can spontaneously self-assemble to form two-dimensional, large-area surfaces offer an attractive alternative approach. This is especially true if the proteins either naturally possess or can be engineered to display functional domains/amino acids that can be exploited for the targeted assembly of nanoscale structures, where one example is the use of engineered chaperoning proteins for nanoparticle templating as demonstrated by McMillan et al.[17] Although there are a number of proteins capable of self-assembly, one exceptional group are S-layer proteins, which are prokaryotic cell surface-layer proteins capable of forming two-dimensional protein lattices over a large surface area, both in vivo and in vitro.

S-layer protein lattices are found on the outermost surface of many bacteria and are composed of protein (or glycoprotein) monomers with a molecular weight of 40−200 kDa depending on the particular bacterial species. S-layers display a highly repetitive surface structure and typically assemble into oblique (p2), triagonal (p3), square (p4), or hexagonal (p6) monolayer structures that are 5−15 nm thick. The lattice constants can range from 3 to 30 nm, and within the lattice structure itself, pores of identical morphology and size (2−6 nm) are formed[18,19] (Figures 1 and 2). In vivo, one side of the S-layer (inner face) is attached to the cell while the other side (outer face) is exposed to the environment; and there is often a significant difference in the surface topology and physiochemical properties between the two sides.[20] Importantly, a number of S-layer proteins can be extracted, disintegrated into monomers, and then reassembled in vitro onto both planar and three-dimensional substrates.[21] The ability to rebuild the periodic structure of the S-layer (containing within it potential binding sites for different types of molecules and particles) opens the way to a variety of possible biotechnological applications for S-layers.[22,23] Furthermore, the unique surface topography, chemical properties, re-assembly potential,

* Corresponding author. Phone: 607-255-8579. Fax: 607-255-3904. E-mail: mb347@cornell.edu.
† Department of Microbiology.
‡ Alliance for Nanomedical Technologies.

10.1021/jp049280l CCC: $27.50
Published on Web 05/22/2004

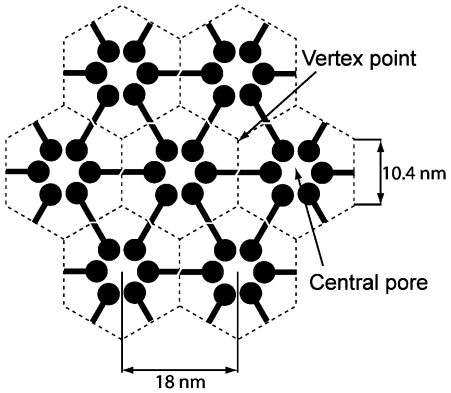

Figure 1. Schematic illustration of the structure and hexagonal (p6) symmetry of the HPI S-layer. In each core unit, six protein monomers surround a ~2.2-nm-diameter central pore. Spoke-like protrusions emanate from each monomer to connect adjacent hexameric units. Dotted lines illustrate a regular hexagonal lattice model overlaid on top of the HPI layer aligned such that (1) the corners of the hexagons correspond to vertex-point regions in the HPI layer, and (2) the geometric center of each hexagon corresponds to the location of the central pore of the S-layer.

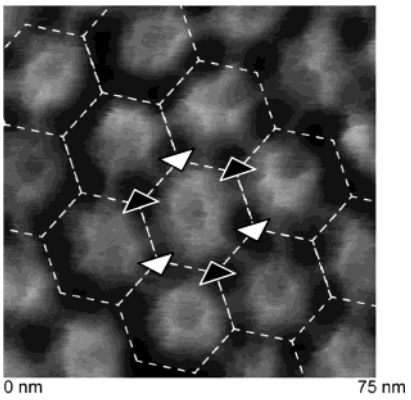

Figure 2. High-resolution AFM image of the intracellular face of the HPI S-layer acquired using a carbon nanotube tip. In this image, the (hexameric) protein core unit as well as the central pore can be visualized. Similar to Figure 1, the dotted hexagonal lattice model is aligned with the vertex-point and central pore regions of the HPI layer. Black and white triangles illustrate the 3-fold symmetry of the vertex points surrounding one core unit.

and highly repetitive structure makes S-layers particularly suitable as biotemplates to fabricate nanostructures and arrays in a parallel fashion. Thus, S-layers have recently been used as ultrahigh-resolution lithographic templates for metallic deposition/ion milling processes,[24−26] electron-induced nanoparticle formation,[27] as well as the mineralization of CdS semiconducting particles.[28] Particles that are formed in situ, using the templating methods listed above, are typically not monodisperse, and the conditions employed for the direct chemical synthesis of such quantum nanostructures in the presence of biological components are not necessarily ideal. An alternative option is to use pre-manufactured nanoparticles and quantum dots (QD's) for S-layer-based arraying applications.[29−31] The use of pre-fabricated (metallic or semiconducting) nanoparticles would allow for better control of particle morphology, and hence result in more homogeneous particle properties and size distributions, which are necessary when measuring, for example, enhanced optical nonlinearity.[32]

One particularly interesting S-layer for nanoparticle templating is the hexagonally packed intermediate (HPI) layer of *Deinococcus radiodurans*, which has a p6 symmetry with a 2.2-nm central pore, and a pore-to-pore distance of 18 nm.[33] In a short communication, Hall and co-workers have demonstrated the ability of HPI to specifically bind citrate-stabilized, gold nanoparticles, resulting in ordered arrays over several hundred nanometers, where the long-range order is influenced by the particle size.[30] Unfortunately, lack of high-resolution 3-D structural data and very limited information about the physical/chemical characteristics of HPI, and S-layer surfaces in general, make it difficult to precisely determine where on the S-layer surface the particles bind and the interactions responsible for the binding. Here, we investigate the interaction of pre-synthesized gold nanoparticles with native HPI layers in order to expand the knowledge base about how such particles interact with HPI surfaces, and also aim to optimize the binding to produce long-range, ordered arrays of nanoparticles which will be useful for future optical investigations.

Materials and Methods

Chemicals and Materials. α-Tolulene sulfonyl fluoride (Acros), dichlorodimethylsilane (Gelest), ethanol (Aldrich), lithium dodecyl sulfate (Sigma), mercaptoundecanoic acid (Sigma), mercaptohexadecanoic acid (Sigma), mercaptoundecanol (Sigma), sodium chloride (Sigma), tri-sodium citrate (Sigma), Triton X-100 (Sigma), ultrapure 18.2 MΩ DI H_2O (Stephens Scientific Co., NJ), 5-nm Au nanoparticles (British Biocell, UK), and silica (SiO_2)- and carbon-coated transmission electron microscopy (TEM) grids (SPI supplies). All chemicals were of A.C.S. reagent grade or better, and all other materials were used as received unless otherwise stated.

Bacterial Culture Conditions and HPI Layer Purification. *Deinococcus radiodurans* (Sark I strain) was cultured in TGYM media at 30 °C to an OD_{600} ~ 0.5 and subsequently harvested by centrifugation at 5000G for 90 min at 4 °C. After the initial centrifugation, the cells were washed twice by resuspension in 0.1 M NaCl/1 mM α-toluene sulfonyl fluoride (PMSF), followed by centrifugation as above. After the last centrifugation, the cells were resuspended in DI water supplemented with 1mM PMSF in a volume 20 times the cell pellet volume. Extraction of HPI S-layer sheets from the intact cells was performed according to a protocol described by Baumeister et al.,[34] where lithium dodecyl sulfate (LDS) was added to the resuspended cells to 2% and extracted at 4 °C for 4 h. After extraction, cells were removed by centrifugation at 2500G for 20 min and the HPI sheets subsequently pelleted by a 20000G spin for 30 min at 4 °C. HPI sheets were washed 3 times in 1 mL of 2% LDS, 0.1 mM PMSF, and then an additional 6 times in 1 mL of DI water by repeated resuspension−centrifugation at 20000G as above. The HPI stock solution (~0.5 mg/mL protein in ultrapure DI water) was stored at 4 °C until further use.

Preparation of TEM Grids. Silica-coated TEM grids were cleaned for 1 min at high power (29.6 W) in a benchtop air plasma cleaner (Harrick Scientific, NY) to render the grids hydrophilic. After plasma treatment, the grids were either used for HPI adsorption immediately or derivatized with dimethyldichlorosilane (DDS) using a gas-phase derivatization method where 10 μL of saturated DDS vapor were injected into an airtight vessel containing freshly cleaned SiO_2−TEM grids and left to react for 45 min at 25 °C. This generates a highly hydrophobic, methylated SiO_2 surface.[35] Carbon-coated TEM grids were used as received.

Derivatization of Au Nanoparticles. Ligand-exchange reactions of citrate-stabilized 5-nm Au nanoparticles were performed similarly as described by Weisbecker et al.[36] with either mercaptoundecanoic acid ($HS(CH_2)_{10}COOH$), mercaptoundecanol ($HS(CH_2)_{11}OH$), or mercaptohexadecanoic acid

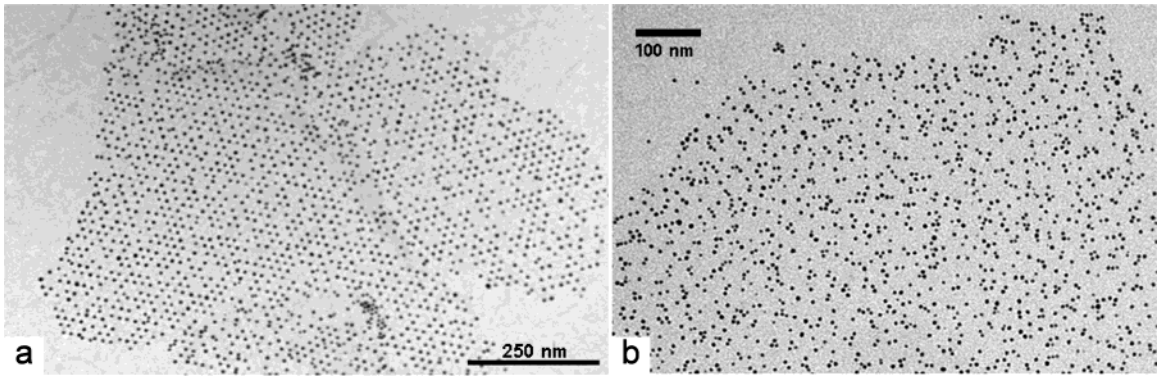

Figure 3. TEM images illustrating the two types of patterns observed when 5-nm citrate-capped gold nanoparticles are adsorbed onto the surface of *D. radiodurans* HPI S-layers. (a) Long-range ordered pattern. (b) Random-adsorption pattern.

($HS(CH_2)_{15}COOH$). A quantity of 2 μL of 25 mM thiol in ethanol was added to 1 mL of 5-nm citrate-stabilized gold particles (80 nM) and incubated with continuous agitation at 25 °C for 16 h (0.05% (w/v) TRITON X-100 was added to the mercaptoundecanol reaction to prevent particle aggregation). After derivatization of the gold particles with the respective ligands, the solutions were dialyzed against DI water using regenerated cellulose membranes (10 kDa MW cutoff, Sigma) for 2−4 h at room temperature. The particles were used immediately after the dialysis procedure.

HPI Adsorption to TEM Grids and Templating of Au Nanoparticles. HPI sheets were diluted to a concentration of 50 μg/mL in 10 mM sodium citrate buffer, pH 8.5. SiO_2, DDS, and carbon-coated TEM grids were floated separately on top of 50-μL drops of the HPI solution for 1 h and subsequently rinsed by consecutively floating each grid on 10 separate 50-μL drops of DI H_2O (30 s each wash). Immediately after the rinsing steps, each grid was floated onto a 50-μL drop of citrate-stabilized or ligand-exchanged 5-nm Au nanoparticles (80 nM). After 30 min, 1.5-μL aliquots of a NaCl stock solution were injected into selected samples of each grid type to a final concentration of 25 mM; adsorption of the Au particles was then allowed to continue on all grids for an additional 15 min. Multiple rinsing steps in DI H_2O to removed loosely adsorbed nanoparticles were performed as above. In the instances where negative staining was used, the samples were floated for 1 min on a 2% uranyl acetate solution immediately after DI H_2O rinsing. Samples were blot-dried using filter paper and imaged in a Morgagni Transmission Electron Microscope (Philips) operated at 80 kV.

All image analyses were performed using ImageJ, a java-based software developed by NIH (http://rsb.info.nih.gov/ij/). Particle−particle distance measurements were performed on a selected area of a HPI layer containing a minimum of 100 particles showing a long-range order. The center (x,y) coordinates for each particle were then used to calculate the distance between adjacent particles. Particle surface coverage measurements were carried out by first defining a region of interest on the HPI layer, and then performing a grain analysis to quantitate the number of particles per μm^2. Results presented are mean values (± standard deviation) derived from triplicate experiments, where the calculated surface coverage values were obtained by analyzing nanoparticle adsorption data spanning a combined total area of at least 200 μm^2.

Results and Discussion

The HPI layer from *D. radiodurans* consists of a monomeric protein, about 100 kDa in MW, where six protein monomers in a p6 symmetry form a basic hexameric core unit with a central pore (Figure 1). Both TEM and atomic force microscopy (AFM) studies of the HPI layer have shown that spoke-like structures protrude from the core and connect adjacent units, creating a 2-D hexagonal lattice with a pore-to pore spacing of 18 nm (Figures 1 and 2).[33,37] Six relatively large openings displaying 3-fold symmetry, referred to here as vertex points regions, are symmetrically arranged around the hexameric protein core (Figures 1 and 2). The central pore has a conical shape with a somewhat larger opening on the outer (extracellular) face and a diameter of ~2.2 nm. The surface topography of the outer face is "smoother" than the inner (intracellular) face, which appears more rugged in TEM and AFM.[33,34,38] The N-terminus of the HPI protein has been shown to covalently bind phospholipids, which are believed to be involved in the anchoring of the HPI layer to the cell. The side of HPI that anchors to the cell (the inner face) is considered hydrophobic, while the part of HPI that faces the external environment (the outer face) is generally regarded as hydrophilic.[37] Although the last 50 amino acids of the C-terminus are known to contain many polar groups and aromatic amino acids, there is a lack of detailed information on localized charge distributions and hydrophobic properties, as no high-resolution 3-D structure of the HPI-layer protein is currently available. To date, only a low-resolution structure has been elucidated through image reconstruction of transmission electron microscopy tilt series.[33]

The biotemplating of citrate-capped Au nanoparticles using HPI S-layers results in the specific adsorption of the particles to the isolated protein sheets. Typically two distinct patterns of adsorption can be visualized: first, a long-range ordered pattern that spans most of the HPI sheet (Figure 3a); and second, a more random appearing adsorption pattern with subtle indications of an underlying, ordered structure (Figure 3b). The occurrence of these two types of patterns is most probably due to intrinsic differences in the biochemical/biophysical properties of the two faces of the HPI layer, such that different templating properties are observed depending on which face of the HPI fragment is oriented upward toward the nanoparticle solution. For the most part, the extracted HPI fragments adsorbed either as large-area monolayer sheets or as partial double layers, as confirmed by AFM using mica and silica substrates, and presumably similar adsorption occurs on the TEM grids. Particle adsorption onto the partial double-layer sheets displayed both an ordered and random pattern (as seen in Figure 5a). As our main interest lies in the ability of HPI layers to promote the creation of ordered nanoparticle arrays, we shall focus on our results concerning ordered-pattern formation and discuss how such patterns are formed in a reproducible manner.

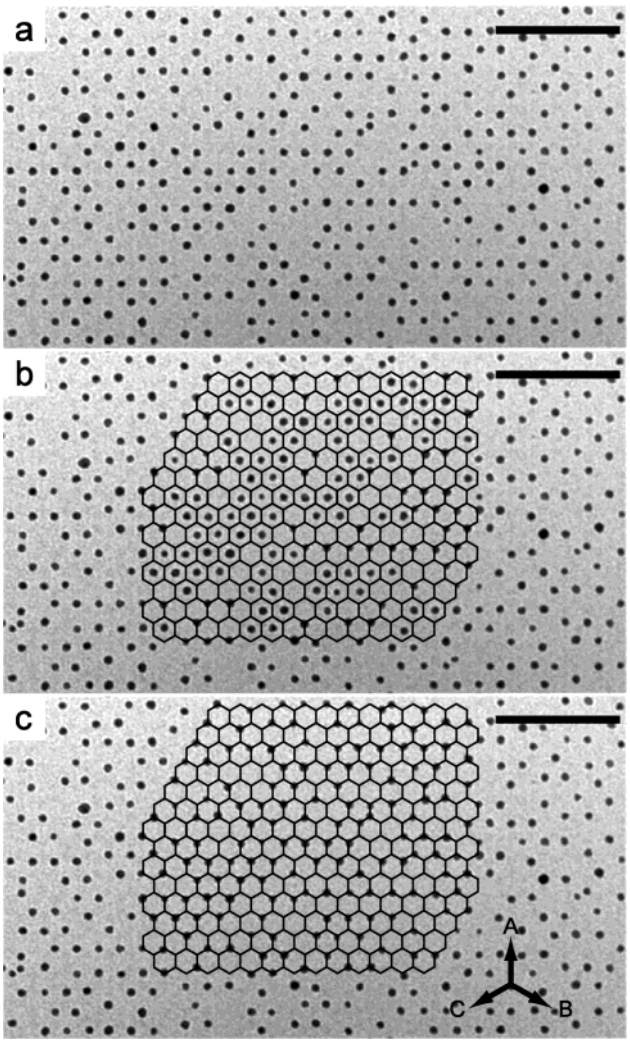

Figure 4. Illustration of two alternative models for the localization of gold nanoparticles adsorbed onto HPI S-layers without addition of 25 mM NaCl. Scale bars = 100 nm. (a) TEM image showing the hexagonal packing of gold particles on the HPI surface. (b) Overlay of an ideal hexagonal lattice template according to a central pore-adsorption model. In this model, a large number of apparently "misaligned" particles (which instead overlap with the vertex regions) can be clearly seen. (c) Overlay of an ideal hexagonal lattice template according to a vertex point-adsorption model where, compared to the case shown in (b), the hexagonal lattice template has been shifted upward 10.4 nm along vector *A*. The particles appear to be in perfect register with the lattice template.

TABLE 1: Number of Nanoparticles Adsorbed onto HPI Layers Using Different Ionic Strength[a]

	ordered pattern particles/μm^2	random pattern particles/μm^2	theoretical value particles/μm^2
0 M NaCl	3100 ± 220	2350 ± 150	3564 (all pore)
25 mM NaCl	6878 ± 398	4870 ± 800	7128 (all vertex)

[a] Theoretical values are calculated assuming a complete, perfect binding of nanoparticles to either the central pore of the HPI layer (all pore) or to the HPI layer vertex points (all vertex).

It should be noted that the carbon-coated TEM grids used for our experiments appeared to be only partially hydrophobic, with variations in the degree of hydrophobicity between different grids. On these particular grids the HPI sheets adsorbed in such a way that both random and ordered nanoparticle patterns were obtained, with the random adsorption patterns observed frequently. Due to the variations in surface properties observed between individual grids, no measurement results or discussion regarding the templating of nanoparticles on HPI sheets preadsorbed onto carbon-coated grids have been included in the present paper.

TABLE 2: Interparticle Distance on Ordered Nanoparticle Patterns Formed on HPI Layers

	interparticle distance (nm)
0 M NaCl	18.1 ± 0.7
25 mM NaCl	10.4 ± 0.8

Au Nanoparticles Templated on HPI Adsorbed to Hydrophobic DDS Surfaces. A large number of the HPI layer sheets adsorbed to DDS surfaces displayed a long-range, hexagonally ordered adsorption pattern when incubated with the citrate-capped Au nanoparticles in the absence of NaCl (Figures 3a, 4a). This long-range patterning is comparable to the results reported previously by Hall et al., where HPI layers were initially adsorbed to carbon TEM grids and subsequently templated with Au nanoparticles.[30] This site-specific adsorption has been postulated to occur within the central pore of the outer face of the HPI layer through charge−charge interactions, such that the resulting interparticle spacing corresponds directly with the pore-to-pore spacing of the HPI layer. This adsorption model would result in a uniform hexagonal-packed nanoparticle pattern over the whole HPI sheet with an ideal particle spacing of 18 nm and a theoretical surface coverage of 3564 particles/μm^2 (i.e., 1 particle adsorbed in a regular hexagon enclosing a surface area of 280.6 nm^2) (Table 1). The empirically determined surface coverage of the long-range ordered patterns seen on the DDS surfaces is 3100 ± 220 particles/μm^2 with a particle−particle distance of 18.1 ± 0.7 nm (Table 2). This result comes close to the calculated values for ideal pore adsorption. However, upon closer inspection, slight mismatches (or misalignments) can be seen in the long-range order if one adheres strictly to a pore-only adsorption mechanism. These mismatch sites are more easily discerned by projecting an extended hexagonal model lattice template over the TEM images. The lattice template has the same symmetry as the HPI layer and is defined in Figures 1 and 2. By visually positioning the lattice template to correspond with a "pore-only" adsorption model, misaligned particles are obvious (Figure 4b). On the other hand, when the overlaying lattice template is translated 10.4 nm (along any of the model lattice vectors) to correspond with a vertex point adsorption model, the particle arrangement is in good agreement with the theoretical lattice (Figure 4c). This observation suggests that nanoparticle adsorption on the HPI layers may in fact occur at the vertex regions, and not within the central pore. Due to the symmetrical structure of the HPI layer, the binding of particles to every second vertex point would give the same physical pattern (with respect to particle spacing and surface coverage) as adsorption to the central pores (Figure 7).

Upon introducing NaCl to the nanoparticle solution, there is a dramatic increase in the overall level of adsorption of nanoparticles to the HPI surface. This increase is accompanied by the formation of a visually striking honeycomb pattern over the entire HPI sheet, which provides strong evidence for a vertex point adsorption model (Figure 5a,b). Occasionally, some unfilled vertices are observed, most likely corresponding to sites blocked by contaminant debris seen to reside on the extracted HPI layers using AFM (not shown). The surface coverage for the long-range ordered pattern is 6878 ± 398 particles/μm^2 and the interparticle distance is 10.4 ± 0.8 nm (Tables 1 and 2). The results agree well with the theoretical vertex−vertex point distance of the HPI lattice (10.4 nm) and come close to the expected value of 7128 particles/μm^2 for the situation where all the vertex points of the HPI layer are occupied with particles

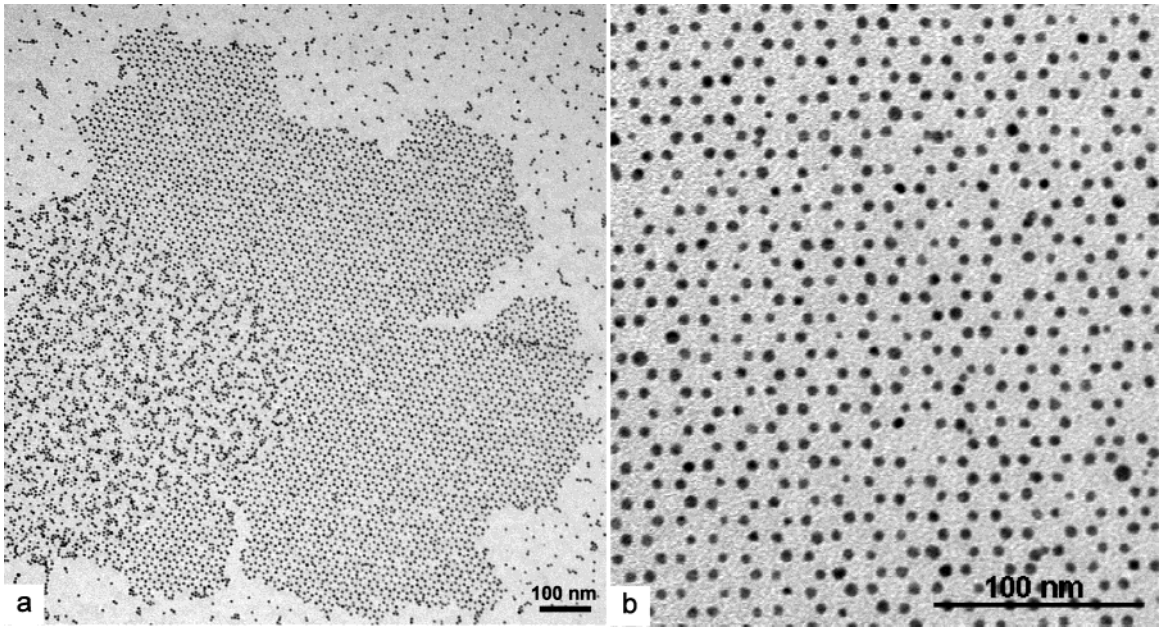

Figure 5. Illustration of the effect of increased ionic strength on the adsorption of citrate-capped gold nanoparticles on HPI S-layers. (a) Long-range ordered adsorption pattern obtained upon addition of 25 mM NaCl to the nanoparticle solution. On the partial double-layer fragment shown here, the occurrence of a random-adsorption pattern can also be seen on the left side of the image. (b) Higher magnification of the long-range ordered honeycomb pattern formed on the HPI layers.

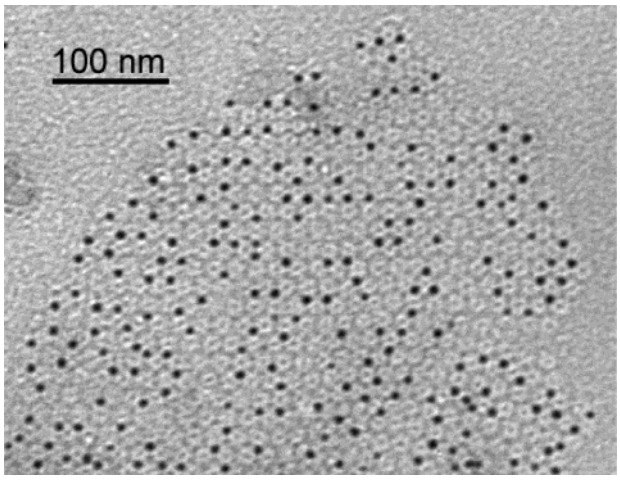

Figure 6. Gold nanoparticles adsorbed to HPI layer without addition of 25 mM NaCl and then stained with 2% uranyl acetate. The individual hexameric core units are easily discerned and adsorption to vertex points is evident.

(Table 1). To visually confirm that vertex point adsorption is taking place, HPI samples were prepared and negatively stained after adsorbing the nanoparticles, without the addition of NaCl. The results clearly show that adsorption occurs at the vertex points of the ordered patterned regions (Figure 6). It is interesting to note that the addition of NaCl directly to the nanoparticle solution prior to incubation with the HPI layer sheets generally results in adsorption patterns that display much less spatially defined long-range order. In addition, a higher overall amount of particle aggregation on the HPI layer is obtained.

As the inner face of the HPI layer is hydrophobic,[37,38] it is most likely that this face is adsorbed directly to the hydrophobic DDS surfaces, such that the outer face is exposed toward the nanoparticle solution. The preferential orientation of the HPI inner face toward hydrophobic substrates has been demonstrated previously using AFM, where isolated HPI fragments were adsorbed to highly ordered pyrolytic graphite (HOPG) and other types of hydrophobic surfaces.[39,40] The above observations suggest that the ordered array pattern (as exemplified by Figure 4a) probably occurs via adsorption of the gold nanoparticles to the outside face of the HPI sheets.

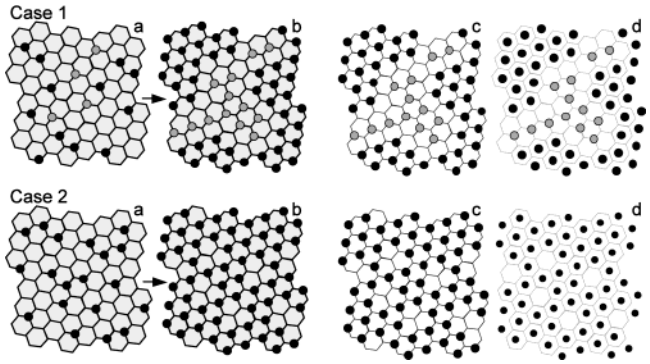

Figure 7. Schematic illustration of the hypothetical progression of nanoparticles binding to the vertex point regions of the HPI S-layer. Different adsorption patterns arise, depending on the initial adsorption of particles relative to each other. Gray dots represent particles adsorbed at vertices located an *odd* number of vertex points away from particles represented by black dots. Light-gray filled honeycomb pattern represents the hexagonal S-layer protein sheet where (a) and (b) represent earlier and later phases of nanoparticle adsorption, respectively. Dark-gray hexagonal lattices (c) represent the alignment of a lattice template corresponding to a vertex point adsorption model. Light-gray hexagonal lattices (d) represent the alignment of a lattice template corresponding to a pore-adsorption model. Case 1: Nanoparticles represented by gray dots adsorb in such a way that other nanoparticles (black dots) are located an *odd* number of vertex points away from them. Using a vertex-point adsorption model (c), no apparently "misaligned" particles are visible. However, when using a pore-adsorption model the gray particles appear to be "misaligned" relative to the black particles (d). Case 2: All nanoparticles adsorb an *even* number of vertex points away from other nanoparticles on the S-layer protein sheet. In this case, no apparently "misaligned" particles are visible when either the vertex-point adsorption model lattice template (c) or the pore-adsorption model lattice template (d) are overlaid.

Au Nanoparticles Templated on HPI Adsorbed to Hydrophilic SiO_2 Surfaces. HPI layer sheets that were preadsorbed

to underivatized, hydrophilic SiO_2 TEM grids and then used to template citrate-capped Au nanoparticles in the absence of NaCl displayed a random adsorption pattern with a nanoparticle surface density value of 2350 ± 150 particles/μm^2 (Figure 3b, Table 1). Even though there is no obvious long-range order, the observation that there is a preferential adsorption of nanoparticles to the HPI protein sheets (versus the TEM grid surface itself) is indicative of some sort of selective interaction. Although no major difference in the particle adsorption pattern could be seen upon injecting NaCl into the nanoparticle solution, the amount of surface coverage did increase significantly to 4870 ± 800 particles/μm^2 (Table 1). As the outer surface of HPI is hydrophilic, the adsorption of S-layer sheets onto hydrophilic surfaces preferentially occurs with the outer face oriented toward the surface, (as confirmed through AFM studies by Müller et al.;[41] and also observed by us during our AFM experiments), and the inner face exposed toward the colloid solution. Although negative staining of HPI samples adsorbed onto SiO_2 TEM grids and then exposed to the nanoparticle solution gave a only a faint contrast, it was still possible to discern that adsorption to both vertex points and pores occurred on the S-layer samples (Figure S1).

Since both faces of the HPI layer apparently display some affinity for binding negatively charged gold particles, and because our attempts to stain HPI sheets containing such adsorbed particles have been unable to produce unambiguous molecular structure data in fine detail, it is challenging to try to ascertain on which face of the HPI layer the ordered adsorption process actually occurs. However, the hypothesis that ordered particle binding occurs to the outside face is supported by the observation that there is a greater number of ordered patterns on the hydrophobic DDS surfaces, since HPI layers have been shown to adsorb to such surfaces with their hydrophobic inner face. Moreover, given that it has been argued that site-specific adsorption occurs through electrostatic interactions, it is likely that particle binding occurs on the outer face,[30] since the majority of the charged amino acids of the HPI protein monomer are located in the C-terminus, which is believed to be located on the outer face.[37] Conversely, the random-appearing adsorption pattern presumably corresponds to particle adsorption taking place on the HPI inner face.

Ordered Nanoparticle Patterns on HPI Layers, Sparse vs Dense-Packing. As shown in the previous section, the long-range ordered, hexagonal packing of gold particles to the outer face of HPI layers can take place either in the presence or absence of NaCl addition to the colloid solution. In either case, the adsorption of the nanoparticles appears to preferentially occur at the vertex points of the HPI layer. Since the HPI layer's intrinsic charge distribution is expected to be symmetrical, and because each of the vertex points should have an equal probability of binding particles, the fundamental basis for the occurrence of the two different types of packing densities observed (Figure 4 vs Figure 5b) most likely lies with the net levels of electrostatic repulsion taking place between adjacent particles during the adsorption process.

By employing standard DLVO theory,[42,43] it can be shown that under ionic strength conditions below 1 mM NaCl, the charges present on the surface of the gold nanoparticles used in this study result in a electrostatic double layer that can extend 10 nm or more out from the particle surface. Because electrostatic interactions are more prominent at low ionic strength conditions, as Debye screening effects are reduced, the sparser packing density observed under such conditions is most probably due to interparticle repulsion. In this case, the repulsion leads to nanoparticle adsorption taking place at roughly every second vertex point, and the final pattern therefore ends up mimicking the adsorption pattern that would arise from an all-out central pore adsorption. The occurrence of misaligned particles (illustrated in Figure 4b by overlaying a lattice model displaying perfect hexagonal packing) is likely dependent on where initial adsorption events take place on the surface of the HPI layer. If most of the initial "nucleation" sites all happen to be in register with each other such that there is an even number of vertex points between them, a much more ordered hexagonal pattern will be obtained (Figure 7). Thus fewer misalignments will be seen in the final pattern.

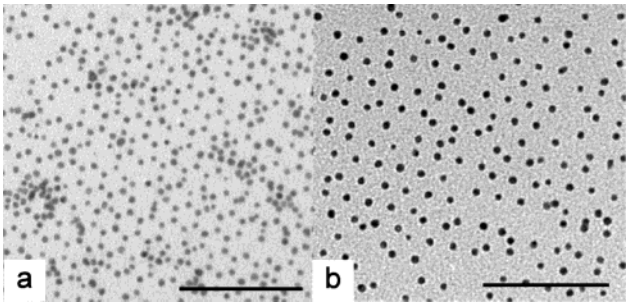

Figure 8. Bio-templating of gold nanoparticles capped with carboxylic acid-terminated alkanethiols. Scale bars = 100 nm. (a) $HS(CH_2)_{10}COOH$-derivatized gold nanoparticles adsorbed onto HPI S-layers in the presence of 25 mM NaCl. A honeycombed ordered pattern can be visualized. (b) $HS(CH_2)_{15}COOH$-derivatized gold nanoparticles adsorbed onto HPI S-layers in the presence of 25 mM NaCl. Compared to the case shown in (a), the packing density of the nanoparticles on the S-layer surface appears to be lower, most likely due to electrostatic/steric repulsion.

To further investigate the role of interparticle interactions in the ordered templating of gold nanoparticles on HPI layers, we used nanoparticles capped with two different types of carboxy-terminated alkanethiol ligands. Specifically, we used 5-nm gold particles derivatized with either mercaptoundecanoic acid ($HS(CH_2)_{10}COOH$) or mercaptohexadecanoic acid ($HS(CH_2)_{15}COOH$). Previously, Porter et al. reported that the thickness of a self-assembled alkanethiol monolayer typically increases with the number of carbons (*n)* as $3.8 + 1.5n$ Å.[44] If we approximate the chain length of our carboxy thiols using this formula, we obtain a monolayer thickness estimate of ~1.9 nm for mercaptoundecanoic acid and ~2.8 nm for mercaptohexanoic acid. Even though the packing might be similar to alkanethiols, the presence of charged and polar headgroups could induce chain disorder and other defects that influence the layer.[45,46] The ζ-potential for monolayers of these molecules has been shown to be about −30 to −40 mV, respectively.[47] Even though more precise data on the particles used here would be desirable, the values stated above provide us with adequate estimates of the chain length/surface potential of the various ligands that are sufficient for this discussion. Given these values, we would expect the physical diameter of 5-nm Au particles coated with $HS(CH_2)_{10}COOH$ to be ~8.8 nm, and ~10.6 nm for particles coated with $HS(CH_2)_{15}COOH$. When these derivatized particles were adsorbed to the HPI layers in the presence of NaCl, the $HS(CH_2)_{10}COOH$-capped particles formed essentially the same type of ordered, close-packed honeycomb pattern as the underivatized (citrate) particles (Figure 8a), whereas the $HS(CH_2)_{15}COOH$-capped particles tended to form the less packed, ordered structure.

In the case of the $HS(CH_2)_{15}COOH$-capped particles, the effective diameter of a single particle is in reality greater than 10.6 nm, given the additional contribution of the electric double layer thickness (i.e., the distance where the surface charge can

affect other particles), which should be in the range of a few nanometers for the ionic strengths used here.[42,43] As the theoretical vertex−vertex distance is 10.4 nm, it is likely that formation of the densely packed pattern by the $HS(CH_2)_{15}$-COOH-capped particles is hindered, even in the presence of salt, due to the electrostatic/steric repulsion that would occur between particles if all vertex points were occupied. It should be acknowledged that with a similar reasoning there would also likely be a slight overlap of the electrical double layers for the $SH(CH_2)_{10}COOH$-capped particles at the ionic strengths used, but as our empirical results clearly demonstrate they are in fact able to form close-packed ordered patterns. Nevertheless, the approximations used for the ligand-capped gold particles support the general concept that the different types of nanoparticle adsorption patterns seen on HPI S-layers is strongly influenced by interparticle repulsion.

Additional studies were also conducted to examine whether the ordered adsorption pattern occurs as a consequence of electrostatic interactions taking place between positive groups on the HPI layer and negative groups on the gold particles. For these investigations, we performed adsorption experiments using positively charged polycationized ferritin (PCF) protein molecules, as well as gold particles derivatized with mercaptoundecanol ($HS(CH_2)_{11}OH$), rendering them hydrophilic but uncharged. The results of these control experiments showed that virtually no particles of either PCF or Au capped with $HS(CH_2)_{11}OH$ adsorbed onto the HPI layers (Figure S2, S3). Taken together, the above findings suggest that the site-specific, spatially ordered adsorption of Au nanoparticles onto HPI surfaces occurs at the vertex points located on the outside face of the S-layer via electrostatic interactions. Furthermore, our results demonstrate that electrostatic repulsion forces between neighboring particles influence the final interparticle distance, even though the overall symmetry of the adsorption pattern is decided by the structure of the S-layer.

Conclusion

Harnessing nature's ability to form self-assembled structures for novel engineering and biotechnology applications is an attractive alternative to conventional fabrication methods. The HPI layer from *Deinococcus radiodurans*, previously demonstrated to be able to specifically bind negatively charged gold nanoparticles, is herein investigated further as a potential biotemplating surface for synthesis of ordered nanostructured arrays. We show that although specific adsorption of gold nanoparticles occurs on both the intracellular and extracellular faces of extracted HPI fragments, a long-range ordered pattern is only seen on one side, presumed here to correspond to the extracellular face.

The templating of gold nanoparticles on the HPI S-layers under low ionic strength typically resulted in hexagonal-packed ordered arrays with ∼18-nm interparticle spacings. Nanoparticle binding takes place at the vertex points on the HPI layer and, due to the presence of interparticle repulsion forces, adsorption tends to be at every second vertex point. Upon increasing the ionic strength the interparticle repulsions become less prominent, allowing the adsorption of nanoparticles to occur in virtually every available vertex point. This results in the formation of a honeycomb pattern of nanoparticles extending throughout the HPI monolayer sheet. The influence of interparticle electrostatic/steric repulsions were also demonstrated using gold nanoparticles derivatized with carboxy-terminated alkanethiols with different chain lengths. The specific interactions responsible for the binding of negatively charged gold nanoparticles to the HPI surface appear to be electrostatic in nature, since neither uncharged hydroxy-terminated particles nor positively charged ferritin molecules were adsorbed onto the S-layer.

In summary, the templating of gold particles under low ionic strength conditions results in ordered hexagonal arrays displaying various misalignments and deviations away from a perfect hexagonal lattice model. Thus, the repeatable synthesis of large-area, perfectly ordered nanoarrays under such conditions remains a technical challenge. On the other hand, templating the particles under higher ionic strength conditions leads to the facile generation of a densely packed, honeycomb pattern that is highly reproducible and covers the entire surface of HPI fragments in a much more uniform manner. We anticipate that bio-inspired ordered-array structures such as these will be useful to investigate enhanced optical nonlinearity effects and in the future development of novel types of surfaces for electronic, optical, and sensor applications.

Acknowledgment. Many thanks to Dr. Changcheng Zhu for useful nanoparticle discussions. Also extended greetings to all the people working in the Angert and Batt laboratories. This work was supported in part by the Nanobiotechnology Center (NBTC), an STC Program of the National Science Foundation under Agreement No. ECS-9876771, and by the New York State Office of Science, Technology and Academic Research (NYSTAR) through the Alliance for Nanomedical Technologies, a New York State Center for Advanced Technology (CAT) program.

Supporting Information Available: Three figures: gold nanoparticles adsorbed in a random pattern on HPI layers, a control experiment where polycationized ferritin (PCF) was adsorbed to HPI layers, and a control experiment where hydrophilic $HS(CH_2)_{11}OH$-derivatized gold nanoparticles were adsorbed to HPI layers.

References and Notes

(1) Markovich, G.; Collier, C. P.; Henrichs, S. E.; Remacle, F.; Levine, R. D.; Heath, J. R. *Acc. Chem. Res.* **1999**, *32*, 415−423.

(2) Brust, M.; Kiely, C. J. *Colloids Surfaces, A: Physicochemical and Engineering Aspects* **2002**, *202*, 175−186.

(3) Murray, C. B.; Kagan, C. R.; Bawendi, M. G. *Annu. Rev. Mater. Sci.* **2000**, *30*, 545−610.

(4) Guarini, K. W.; Black, C. T.; Zhang, Y.; Kim, H.; Sikorski, E. M.; Babich, I. V. *J. Vac. Sci. Technol., B: Microelectronics and Nanometer Structures* **2002**, *20*, 2788−2792.

(5) Fu, J.; Feng, X.; Han, Y.; Pan, C.; Yang, Y.; Li, B. *Macromol. Rapid Commun.* **2003**, *24*, 487−491.

(6) Park, M.; Adamson, D. H.; Chaikin, P. M.; Register, R. A. *Polym. Mater. Sci. Eng.* **1999**, *81*, 12−15.

(7) Teranishi, T. *Comptes Rendus Chimie* **2003**, *6*, 979−987.

(8) Foerster, S.; Antonietti, M. *Adv. Mater. (Weinheim, Germany)* **1998**, *10*, 195−217.

(9) Lazzari, M.; Lopez-Quintela, M. A. *Adv. Mater. (Weinheim, Germany)* **2003**, *15*, 1583−1594.

(10) Boyen, H.-G.; Kastle, G.; Zurn, K.; Herzog, T.; Weigl, F.; Ziemann, P.; Mayer, O.; Jerome, C.; Moller, M.; Spatz, J. P.; Garnier, M. G.; Oelhafen, P. *Adv. Functional Mater.* **2003**, *13*, 359−364.

(11) Nakao, H.; Shiigi, H.; Yamamoto, Y.; Tokonami, S.; Nagaoka, T.; Sugiyama, S.; Ohtani, T. *Nano Lett.* **2003**, *3*, 1391−1394.

(12) McNally, H.; Pingle, M.; Lee, S. W.; Guo, D.; Bergstrom, D. E.; Bashir, R. *Appl. Surf. Sci.* **2003**, *214*, 109−119.

(13) Xiao, S.; Liu, F.; Rosen, A. E.; Hainfeld, J. F.; Seeman, N. C.; Musier-Forsyth, K.; Kiehl, R. A. *J. Nanoparticle Res.* **2002**, *4*, 313−317.

(14) Mayes, E.; Bewick, A.; Gleeson, D.; Hoinville, J.; Jones, R.; Kasyutich, O.; Nartowski, A.; Warne, B.; Wiggins, J.; Wong, K. K. W. *IEEE Trans. Magn.* **2003**, *39*, 624−627.

(15) Lee, S.-W.; Mao, C.; Flynn, C. E.; Belcher, A. M. *Science* **2002**, *296*, 892−895.

(16) Baumeister, W.; Barth, M.; Hegerl, R.; Guckenberger, R.; Hahn, M.; Saxton, W. O. *J. Mol. Biol.* **1986**, *187*, 241-250.

(17) McMillan, R. A.; Paavola, C. D.; Howard, J.; Chan, S. L.; Zaluzec, N. J.; Trent, J. D. *Nat. Mater.* **2002**, *1*, 247−252.
(18) Sleytr, U. B.; Sara, M.; Pum, D.; Schuster, B. *Prog. Surf. Sci.* **2001**, *68*, 231−278.
(19) Sleyter, U. B.; Sára, M.; Pum, D. Crystalline Bacterial Cell Surface Layers (S−Layers): A Versatile Self-Assembly System. In *Supramolecular Polymers*; Ciferri, A., Ed.; Marcel Dekker: New York, 2000; pp 177−213.
(20) Sleyter, U. B.; Messner, P.; Pum, D.; Sára, M. *Angew. Chem., Int. Ed. Engl.* **1999**, *38*, 1034−1054.
(21) Sleytr, U. B.; Gyorvary, E.; Pum, D. *Prog. Org. Coatings* **2003**, *47*, 279−287.
(22) Pum, D.; Neubauer, A.; Gyorvary, E.; Sara, M.; Sleytr, U. B. *Nanotechnology* **2000**, *11*, 100−107.
(23) Pum, D.; Sleytr, U. B. *Trends Biotechnol.* **1999**, *17*, 8−12.
(24) Malkinski, L.; Camley, R. E.; Celinski, Z.; Winningham, T. A.; Whipple, S. G.; Douglas, K. *J. Appl. Phys.* **2003**, *93*, 7325−7327.
(25) Moore, J. T.; Beale, P. D.; Winningham, T. A.; Douglas, K. *Appl. Phys. Lett.* **1997**, *71*, 1264−1266.
(26) Panhorst, M.; Bruckl, H.; Kiefer, B.; Reiss, G.; Santarius, U.; Guckenberger, R. *J. Vac. Sci. Technol. B* **2001**, *19*, 722−724.
(27) Wahl, R.; Mertig, M.; Raff, J.; Selenska-Pobell, S.; Pompe, W. *Adv. Mater.* **2001**, *13*, 736−740.
(28) Shenton, W.; Pum, D.; Sleytr, U. B.; Mann, S. *Nature (London)* **1997**, *389*, 585−587.
(29) Messner, P.; Pum, D.; Sara, M.; Stetter, K. O.; Sleytr, U. B. *J. Bacteriol.* **1986**, *166*, 1046−54.
(30) Hall, S. R.; Shenton, W.; Engelhardt, H.; Mann, S. *ChemPhysChem* **2001**, *2*, 184−186.
(31) Gyöervary, E.; Schroedter, A.; Talapin, D. V.; Weller, H.; Pum, D.; Sleyter, U. B. *J. Nanosci. Nanotechnol.* **2004**, *4*.
(32) Takagahara, T. *Surf. Sci.* **1992**, *267*, 310−14.
(33) Baumeister, W.; Barth, M.; Hegerl, R.; Guckenberger, R.; Hahn, M.; Saxton, W. O. *J. Mol. Biol.* **1986**, *187*, 241−50. FIELD Reference Number: FIELD Journal Code: 2985088R FIELD Call Number:.
(34) Baumeister, W.; Karrenberg, F.; Rachel, R.; Engel, A.; Ten Heggeler, B.; Saxton, O. W. *Eur. J. Biochem.* **1982**, *125*, 535−544.
(35) Bergkvist, M.; Carlsson, J.; Oscarsson, S. *J. Biomed. Mater. Res.* **2003**, *64A*, 349−356.
(36) Weisbecker, C. S.; Merritt, M. V.; Whitesides, G. M. *Langmuir* **1996**, *12*, 3763−3772.
(37) Peters, J.; Peters, M.; Lottspeich, F.; Schäfer, W.; Baumeister, W. *J. Bacteriol.* **1987**, *169*, 5216−5223.
(38) Muller, D. J.; Baumeister, W.; Engel, A. *PNAS* **1999**, *96*, 13170−13174.
(39) Möller, C.; Allen, M.; Elings, V.; Engel, A.; Müller, D. J. *Biophys. J.* **1999**, *77*, 1150−1158.
(40) Karrasch, S.; Dolder, M.; Schabert, F.; Ramsden, J.; Engel, A. *Biophys. J.* **1993**, *65*, 2437−2446.
(41) Müller, D. J.; Baumeister, W.; Engel, A. *J. Bacteriol.* **1996**, *178*, 3025−3030.
(42) Overbeek, J. T. G. The interaction between colloidal particles. In *Colloid Science*; Kruyt, H. R., Ed.; Elsevier: Amsterdam, 1952; Vol. 1, pp 245−277.
(43) Overbeek, J. T. G. Electrochemistry of Double layers. In *Colloid Science*; Kruyt, H. R., Ed.; Elsevier: Amsterdam, 1952; Vol. 1, pp 115−193.
(44) Porter, M. D.; Bright, J. R.; Allara, D. L.; Chidsey, C. E. D. *J. Am. Chem. Soc.* **1987**, *109*, 3559−3568.
(45) Knez, M.; Sumser, M. P.; Bittner, A. M.; Wege, C.; Jeske, H.; Hoffmann, D. M. P.; Kuhnke, K.; Kern, K. *Langmuir* **2004**, *20*, 441−447.
(46) Schreiber, F. *Prog. Surf. Sci.* **2000**, *65*, 151−256.
(47) Schweiss, R.; Welzel, P. B.; Werner, C.; Knoll, W. *Langmuir* **2001**, *17*, 4304−4311.